

Transition Modelling for Aerodynamic Flow Simulations with a Near-Wall Reynolds-Stress Model

Axel Probst,^{*} Rolf Radespiel,[†]

Institute of Fluid Mechanics, Technische Universität Braunschweig,

38106 Braunschweig, Germany

and Ulrich Rist[‡]

Institute of Aerodynamics and Gas Dynamics, Universität Stuttgart,

70569 Stuttgart, Germany

Abstract

A new approach to model Tollmien-Schlichting-type transition in combination with the Low-Re ε^h -Reynolds-stress model is presented, which relies on additional information from the linear stability analysis performed by an e^N -based transition prediction method. The approach uses eigenfunctions and amplification rates of the velocity fluctuations from stability analysis to provide initial Reynolds-stress and dissipation-rate distributions for the Reynolds-stress turbulence model at the beginning of the turbulent flow regime. The required scaling of the Reynolds stresses is calibrated with the aid of DNS data of a transitional boundary layer with adverse-pressure gradient. The method is successfully applied to a zero- and an adverse-pressure-gradient boundary layer, an airfoil with laminar separation bubble and a 3D flow-through engine nacelle at stall.

Nomenclature

APG	Adverse pressure gradient	$u_i = u, v, w$	Velocity fluctuations
c	Chord length	$ \hat{u}_i $	Amplitude of a TS wave
c_f	Skin friction coefficient	$U_i = U, V, W$	Mean flow velocities
c_p	Pressure coefficient	U_e	Boundary-layer edge velocity
f_0	Frequency for stability analysis	U_∞	Freestream velocity
k	Turbulent kinetic energy	$\overline{u_i u_j}$	Reynolds-stress tensor
N	N factor	TS	Tollmien-Schlichting
N_{crit}	critical N factor	Tu	Turbulence intensity
Re	Reynolds number	x_0	Location for stability analysis
Re_t	Turbulent Reynolds number	x_{tran}	Transition location
$S_{\varepsilon 4}$	Pressure gradient term	z_n	Wall-normal coordinate
S_l	Length scale limiting term		

^{*}Research scientist.

[†]Professor.

[‡]Apl. Professor.

Symbols:		$\tilde{\varepsilon}^h$	Isotropic part of ε^h
α	Angle of attack	ε_{ij}	Dissipation rate tensor
α_i	Spatial amplification rate	φ_{u_i}	Phase shift of a TS wave
ε	Dissipation rate of k	Θ	Circumferential angle
ε^h	Homogeneous part of ε		

1 Introduction

Considering laminar-turbulent transition in numerical simulations of complex aerodynamic flows gained increasing attention in recent years. Although the boundary layers around contemporary transport aircrafts are predominantly turbulent throughout most of the flight regime, the demand for drag reduction has renewed the interest in laminar-flow technologies which require accurate prediction tools in the design phase. Moreover, laminar portions that occur at low Reynolds numbers, e.g. during start/landing phases or in wind-tunnel tests, can significantly influence the stall behaviour of wings and engine nacelles. Treating transition in common RANS (Reynolds-Averaged Navier-Stokes) approaches involves two major aspects: determining the transition location and modelling the laminar-turbulent transition regions.

Apart from simply taking measured values from experiments, the transition location can be derived from empirical correlations [1] which have also been incorporated in complex transport-equation models [2]. Besides, due to its sound physical foundation the semi-empirical e^N method [3], [4] which is aimed to predict Tollmien-Schlichting- and crossflow-type transition, based on linear stability theory, maintains large popularity in the aeronautical community. A recent implementation of the e^N method in the unstructured DLR-TAU code [5] allows for automatic transition prediction even for complex 3D aircraft configurations [6] and constitutes the basis for the present work.

To introduce the transitional effects into the RANS solution, a common approach is to divide the flow domain at the transition point (2D) or line (3D) in order to define a distinct laminar zone, where the modelled turbulence is artificially suppressed [7]. This simple point-transition approach can be extended to include intermittent transition regions by applying additional blending functions [8] or transport equations [2] which are usually intended to slow down the generation of Reynolds stresses at turbulence onset.

However, even without intermittency modelling the computed onset of turbulence is actually often much weaker than in experiments. A common example is transition within laminar separation bubbles which can occur at high angles of attack and low Reynolds numbers: unless specifically tuned to yield enhanced turbulence onset, most common RANS models predict too late reattachment or premature bubble break-up compared to measurements [9].

The shortcomings of point transition have an even stronger impact on low-Re turbulence models with advanced near-wall treatment [10] which are found to delay transition and yield ambiguous transitional behaviour at low freestream turbulence [11]. Recent numerical studies [14] using the low-Re ε^h -RSM [12] broadly confirmed these findings for several aeronautical flow cases. Moreover, a simple ad-hoc remedy based on locally deactivating the near-wall damping was found to affect stall predictions of a flow-through engine nacelle [13].

These observations motivated the development of a new transition modelling approach which aims to consider more of the flow physics in transitional regions in order to provide consistent turbulence onset and to enhance the growth of Reynolds stresses in combination with the low-Re ε^h -RSM. Focusing on Tollmien-Schlichting-type transition for now, the new approach is explained in detail and first applications to flow cases of varying complexity are presented.

2 Numerical Method

2.1 The Low-Re ε^h -Reynolds-Stress Model

The ε^h -Reynolds-stress model [12] specifically accounts for effects of near-wall and non-equilibrium turbulence and has proven to accurately predict flows involving strong pressure gradients and separation [14]. It is based on the Reynolds-stress equations, reading in incompressible form:

$$\frac{D\overline{u_i u_j}}{Dt} = P_{ij} + \Phi_{ij} - \varepsilon_{ij} + D_{ij}^\nu + D_{ij}^t \quad . \quad (1)$$

Only production P_{ij} and viscous diffusion D_{ij}^ν can be computed exactly, whereas the pressure-strain correlation Φ_{ij} , the dissipation rate tensor ε_{ij} and the turbulent diffusion D_{ij}^t require modelling approximations.

In the form presently used the ε^h -RSM employs a linear pressure-strain correlation including the wall-reflection terms Φ_{ij}^w :

$$\Phi_{ij} = -C_1 \varepsilon a_{ij} - C_2 \left(P_{ij} - \frac{2}{3} P_k \delta_{ij} \right) + \Phi_{ij}^w \quad , \quad (2)$$

$$C_1 = C + \sqrt{AE^2} \quad C_2 = 0.8A^{1/2} \quad C = 2.5AF^{1/4}f \quad , \quad (3)$$

$$F = \min(0.6; A_2) \quad f = \min \left[(\text{Re}_t / 150)^{3/2}; 1 \right] \quad . \quad (4)$$

The near-wall damping functions, Eq. (3) and (4), are calibrated based on DNS data and comprise the turbulence Reynolds number Re_t as well as anisotropy invariants of Reynolds stresses (A, A_2) and dissipation rates (E).

The length-scale equation is written in terms of the homogeneous part ε^h instead of the commonly used total dissipation rate $\varepsilon = \varepsilon^h + 1/2 \cdot D^\nu$, as this allows for capturing the correct dissipation rate profile near walls:

$$\frac{D\varepsilon^h}{Dt} = -C_{\varepsilon 1} \frac{\varepsilon^h}{k} \overline{u_i u_j} \frac{\partial U_i}{\partial x_j} - C_{\varepsilon 2} f_\varepsilon \frac{\varepsilon^h \tilde{\varepsilon}^h}{k} + C_{\varepsilon 3} \nu \frac{k}{\varepsilon^h} \overline{u_j u_k} \frac{\partial^2 U_i}{\partial x_j \partial x_l} \frac{\partial^2 U_i}{\partial x_k \partial x_l} + D_{\varepsilon^h} + S_l + S_{\varepsilon 4} \quad . \quad (5)$$

The ε^h -equation is conventionally calibrated with constant coefficients $C_{\varepsilon 1}, C_{\varepsilon 2}, C_{\varepsilon 3}$ and a near-wall damping function f_ε . The length-scale limiter S_l and the pressure-gradient term $S_{\varepsilon 4}$ are additional source terms to sensitize the equation to effects of non-equilibrium turbulence [14]. To finally close the system of equations, the anisotropic dissipation rate tensor ε_{ij}^h is computed via an implicit relation:

$$\varepsilon_{ij}^h = f_s \overline{u_i u_j} \frac{\varepsilon^h}{k} + (1 - f_s) \frac{2}{3} \delta_{ij} \varepsilon^h \quad \text{with} \quad f_s = 1 - \sqrt{AE^2} \quad . \quad (6)$$

2.2 Advanced Transition Modelling

2.2.1 Motivation

The dominant transition type observed on weakly-swept wings and in engine intakes is caused by 2D Tollmien-Schlichting (TS) waves which grow during linear and non-linear amplification stages up to a certain amplitude where breakdown to turbulence occurs. Applying RANS turbulence models to such transitional flows with point transition ignores the whole amplification phase prior to turbulent breakdown. Instead, the model equations, usually only calibrated for

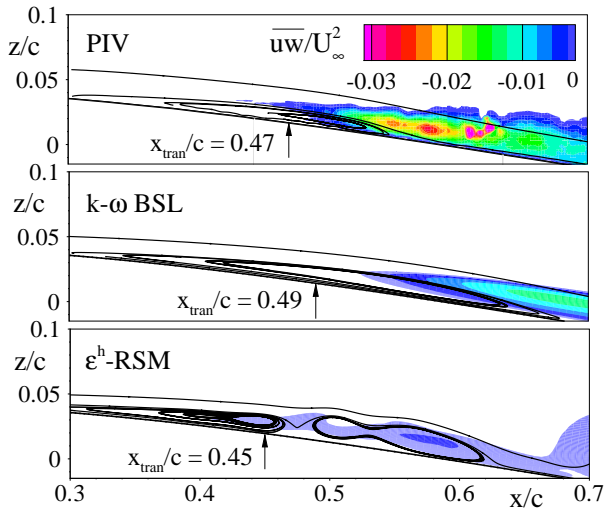


Figure 1: Streamlines and turbulent shear stress on the airfoil SD7003 at $\alpha = 4^\circ$ from experiments [18] and computations with point-transition approach.

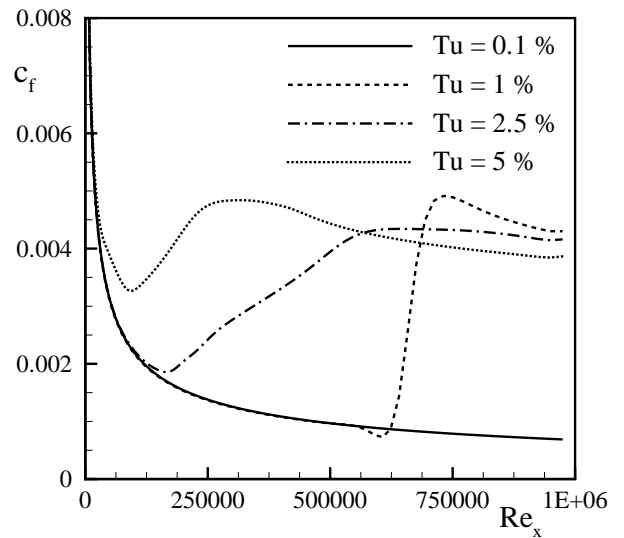


Figure 2: Influence of the freestream turbulent intensity on the transitional behaviour in a “fully-turbulent“ computation of a flat plate flow with the ε^h -RSM.

fully-turbulent flow, are abruptly activated at a certain position within the laminar boundary layer with virtually no modelled turbulence. In the real flow, however, the velocity exhibits considerable fluctuations at this point which formally contribute to the turbulent stresses.

Although the model reaction to simple point transition is rather individual, there are flow cases which clearly illustrate its deficiencies for a wide range of common models. Exemplarily, Fig. 1 compares simulations of the airfoil SD7003 at $Re = 60000$ and $\alpha = 4^\circ$ with corresponding experimental data from a PIV (particle image velocimetry) measurement. This flow exhibits transition within a mid-chord laminar separation bubble, which is modelled in the simulations by the DLR-TAU-code’s e^N -method and the classic point-transition approach. Despite reasonable agreement with the measured transition locations, both the low- Re ε^h -RSM and the $k - \omega$ baseline model [15] clearly underestimate the growth and the maximum level of Reynolds shear stresses downstream of the transition point.

While the “high- Re ”¹ $k - \omega$ baseline model yields a too long, but steady bubble shape, even larger deviations with the ε^h -RSM point out another issue specific to low- Re models which employ damping functions to model near-wall turbulence. As some of these functions depend on the local magnitude of modelled turbulence, such as Eq. (4) in the ε^h -RSM comprising the turbulent Reynolds number Re_t , the damping mechanism can be activated not only close to walls but throughout the whole incoming laminar boundary layer. Thus, even in fully-turbulent mode low- Re models tend to delay transition and reduce the subsequent growth of turbulent stresses. While this feature can be exploited to enable low- Re models to predict bypass transition in environments with high turbulence intensity, it is clearly undesirable in external aerodynamics. As a consequence, a dependency on both the initial conditions and the applied numerical method [11], as well as complete suppression of transition [16] have been reported. For illustration,

¹here, “high- Re ” refers to the absence of any additional damping functions

Fig. 2 shows the results of a series of “fully-turbulent”² computations with the ε^h -RSM of the flat-plate boundary layer with turbulence intensities ranging from $Tu = 0.1\%$ up to $Tu = 5\%$. Early transition is only obtained for very high Tu , whereas at $Tu = 0.1\%$, corresponding to typical low-speed wind-tunnel conditions, no transition at all takes place.

Given the apparent shortcomings of point transition, especially in combination with low-Re turbulence models, we suggest to extend the approach as described in the following sections.

2.2.2 Modelling Approach and Implementation Details

The e^N implementation in the DLR-TAU-code applies the stability solver LILO [19] to compute the amplification rates for a range of disturbance frequencies in the laminar boundary-layer and integrates them along the flow path to obtain the amplitude ratios for each mode, which is commonly expressed in terms of the N-factor, $N = \ln(A/A_0)$. The transition point to activate the RANS model is defined as the location, where the N-factor for the first time exceeds the empirical value N_{crit} [20].

As extension of this approach, the present method is aimed to compute physically valid distributions of Reynolds-averaged turbulent quantities at the end of the linear stage of Tollmien-Schlichting-(TS)-type transition and provide them as local input (“inflow condition“) for the turbulence model. The basic ideas and assumptions are outlined as follows:

- Although the velocity fluctuations in TS waves are not considered “real” turbulence, they can produce Reynolds stresses within the RANS framework and should therefore contribute to a more physical transition behaviour for any RANS model.
- While the shape of the Reynolds stresses in the transition region is determined from the linear stability analysis (Sec. 2.2.3), their absolute magnitudes can only be derived from an empirical calibration (Sec. 2.2.4). The dissipation rate ε required for closure of the equations is computed from the stresses and the spatial amplification rate (Sec. 2.2.5).
- Due to the nature of the linear approach, the present method can only consider the fluctuations at the end of the linear amplification stage, which therefore marks the last point in the laminar zone before activating the turbulence model.
- As the stability analysis is performed in a local, streamline-oriented coordinate system, the computed Reynolds stresses have to be transformed to TAU’s Cartesian system. For the sake of clarity, a special denotation of the streamline-oriented terms is omitted in the following sections.
- In 3D cases the turbulent quantities are only computed at discrete points which are defined by so-called inviscid streamlines. To provide continuous distributions the discrete values are linearly interpolated along the transition line.
- Insertion of the Reynolds-stress and dissipation-rate profiles into the RANS solution is accomplished by additional, local source terms in the turbulence model.
- In line with the e^N implementation in TAU the turbulent input values are evaluated iteratively as addition to each transition-prediction step until converged transition locations and flow solutions are reached.

²i.e., all model terms are fully active in the whole flow domain

2.2.3 Determination of the Reynolds-Stress Shapes

Although the linear stability analysis does not yield any information about the absolute amplitudes of the fluctuations it can still be applied to obtain realistic Reynolds-stress shapes $\overline{u_i u_j}(z_n)$ in dependence of the wall-normal distance z_n because it delivers physically realizable shapes of the fluctuation profiles $u_i(z_n)$.

Following the spatial, linear stability theory of 2D Tollmien-Schlichting waves [17] the fluctuation of any velocity component u_i can be described by the real part of the complex wave ansatz:

$$u_i(z_n) = |\hat{u}_i(z_n)| \cdot e^{-\alpha_i x} \cdot \cos(\alpha_r x - \omega_r t + \varphi_{u_i}(z_n)) , \quad (7)$$

where α_i , α_r , and ω_r are spatial amplification rate, streamwise wavenumber, and frequency, respectively. The only functions of the wall distance z_n in this relation are the amplitudes $|\hat{u}_i|$ and phase shifts φ_{u_i} which can be computed from the real and imaginary parts, \hat{u}_R and \hat{u}_I , of the complex eigenfunctions:

$$|\hat{u}_i| = \sqrt{\hat{u}_{i,R}^2 + \hat{u}_{i,I}^2} \quad , \quad \varphi_{u_i} = \arctan \frac{\hat{u}_{i,I}}{\hat{u}_{i,R}} . \quad (8)$$

These eigenfunctions are the outcome of an additional stability-analysis step with LILO, which is performed at the end of the linear stage, x_0 , for the disturbance mode f_0 which reaches the highest amplification (i.e., the highest value N) at x_0 .

Following the concept of Reynolds averaging, the correlations $u_i \cdot u_j$ given by Eq. (7) are averaged in time at a fixed location (i.e., $\alpha_r x$ can be ignored) while any scaling factors independent of z_n are omitted (i.e., $e^{-\alpha_i x} = 1$). However, as the eigenfunctions obtained from the linear stability equations comprise an undeterminable scaling factor [17], this approach can only provide relations for the shape of the Reynolds-stress profiles, denoted here as $\overline{u_i u_j}^*$:

$$\overline{u_i u_j}^* = \frac{|\hat{u}_i| \cdot |\hat{u}_j|}{2} \cos(\varphi_{u_i} - \varphi_{u_j}) , \quad (9)$$

while obtaining their magnitudes is subject to the following section.

2.2.4 Calibration of the Reynolds-Stress Magnitudes based on DNS data

DNS data of various transitional flows suggest that the fluctuations in TS waves reach a certain saturation amplitude at the end of the linear amplification stage before the rather short stages of non-linear interaction and turbulent breakdown occur [21]. To obtain the scaling of the Reynolds-stress shapes $\overline{u_i u_j}^*$ at that location the present modelling approach involves an additional closure hypothesis: if normalized by a suited integral velocity scale U_{ref} of the local boundary layer profile, the saturation value of the dimensionless amplitude $|\hat{u}_i|/U_{ref}$ is assumed to be universal for TS transition within an acceptable range of uncertainty.

This hypothesis is broadly in line with the basic concept of e^N , as the critical N factor to determine the transition point only reflects the dependency on the initial fluctuation amplitude while the final amplitude at turbulence onset is assumed invariant [20]. Moreover, it is supported by DNS data of different transitional flows [21].

As the universal scaling factor for the (normalized) Reynolds-stress profiles is assumed to only depend on the local velocity scale it can be determined from any suited calibration data set. For this purpose, a DNS of a transitional boundary-layer flow with strong adverse pressure gradient (APG) is selected as reference and as basic validation case [22]. It comprises a Falkner-Skan similarity boundary layer [17] with a Hartree parameter of $\beta = -0.18$. The boundary layer

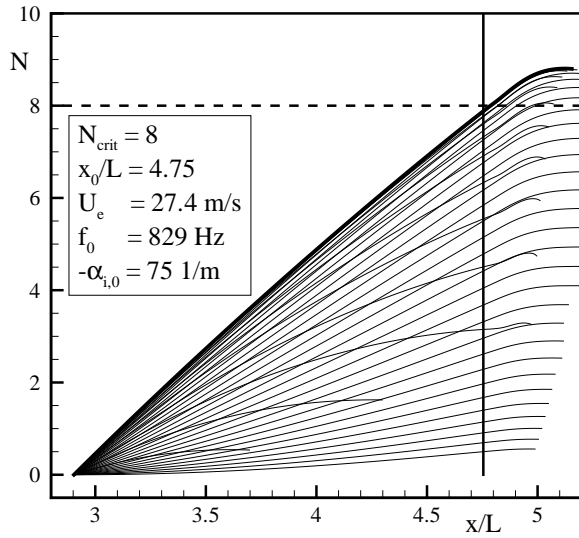


Figure 3: Computed N -factors for different disturbance modes in the APG flow and relevant parameters for the transition model.

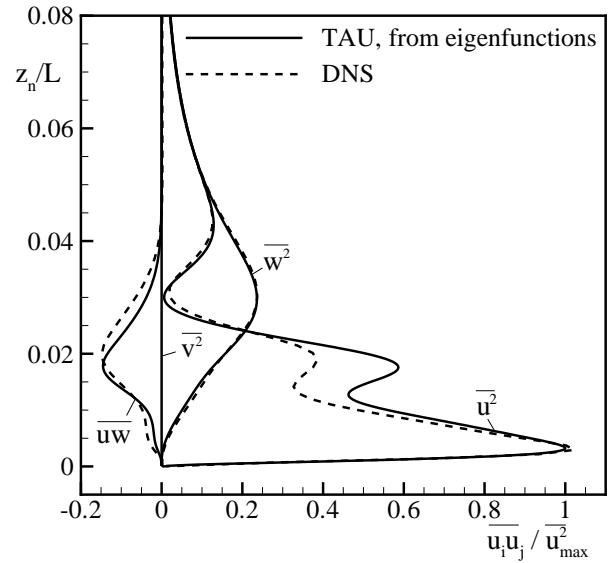


Figure 4: Dimensionless Reynolds stresses at the end of the linear stage in the APG obtained from the eigenfunction analysis in the present model compared to DNS.

undergoes Tollmien-Schlichting-type transition induced by controlled disturbances in the on-flow and can be regarded a characteristic case for a wide range of transitional flows in aircraft aerodynamics.

An N -factor computation based on a laminar TAU solution reveals that the turbulence onset observed in DNS, at about $x_{trans}/L = 4.7$, is approximately matched for $N_{crit} = 8$ (see Fig. 3). For comparison, both the Reynolds-stress distributions evaluated according to Sec. 2.2.3 and the DNS results are normalized with respect to their local maximum values in $\overline{u^2}$. As depicted in Fig. 4, satisfying qualitative agreement is obtained for all Reynolds-stress components supporting the validity of the present approach.

Among several possibilities to characterize the integral boundary-layer velocity we chose the local edge velocity U_e as reference value for the required scaling of the Reynolds stresses. Based on this normalization the DNS data reveals that the maximum value of the streamwise diagonal component of the Reynolds stresses reaches a saturation value of about $\overline{u^2}_{max}/U_e^2 = 0.005$ in the linear stage, or, in terms of wave amplitudes, $|\hat{u}_i|_{max}/U_e = 0.1$. This yields the required scaling of the Reynolds-stress shapes at the end of the linear stage as:

$$\overline{u_i u_j} = 0.005 \cdot U_e^2 \cdot \frac{\overline{u_i u_j}^*}{u_{max}^{2*}} \quad (10)$$

2.2.5 Adjustment of the Dissipation Rate

In order to provide the required input value of the dissipation rate we propose to adjust ε according to the Reynolds stresses and the local spatial amplification rate $\alpha_{i,0}$ of the given mode f_0 at the location x_0 . Written in streamline-oriented coordinates, the amplification rate which is assumed equal for all fluctuation components relates to the Reynolds stresses as:

$$-\alpha_i = \frac{1}{2\overline{u_i u_j}} \frac{\partial \overline{u_i u_j}}{\partial x} \quad (11)$$

Inserting this relation into the Reynolds-stress equations, Eq. (1), and ignoring the negligible contributions of diffusion and redistribution, the dissipation-rate tensor at x_0 can be approximated as:

$$\varepsilon_{ij} = P_{ij} + 2 \cdot \alpha_{i,0} \cdot \left| \vec{U} \right| \cdot \overline{u_i u_j} . \quad (12)$$

As the ε^h -RSM employs just a single equation for the scalar quantity ε^h , Eq. (5), the tensor from Eq. (12) is transformed to the scalar dissipation rate as $\varepsilon = 0.5 \cdot (\varepsilon_{11} + \varepsilon_{22} + \varepsilon_{33})$, before the relation $\varepsilon^h = \varepsilon - 1/2 \cdot D^\nu$ (see Sec. 2.1) is applied.

2.2.6 Modelling Experiences and Practical Implementation

Some shortcomings of the approach should be noted: in some cases, ε^h as derived in Sec. 2.2.5 takes unphysical negative values in the outer part of the boundary layer, which has to be prevented by a limiter. Moreover, due to its calibration for fully-turbulent flow the anisotropy relation Eq. (6) in the ε^h -RSM fails to exactly return the input tensor from Eq. (12).

For that reasons, the desired amplification defined by $\alpha_{i,0}$ cannot be reliably achieved for each Reynolds-stress component. In particular, the considerable shear-stresses observed in flows with adverse-pressure gradients (see Fig. 4) yield large production terms P_{11} for the streamwise diagonal stress which have to be balanced by high values for the respective dissipation-rate component according to Eq. (12). As the diagonal tensor components are lumped into one scalar quantity, ε^h in some cases becomes large enough to actually damp the other stress components, resulting in delayed transition and reduced turbulence onset.

To avoid excessive ε^h values the actual model is modified to consider only the diagonal Reynolds-stress components as local input, whereas the shear stresses in Eq. (10) are set to zero,

$$\overline{u_i u_j} = 0 \quad \text{for } i \neq j \quad , \quad (13)$$

and therefore do not contribute to the dissipation rate as described in Sec. 2.2.5. This remedy was found to ensure sufficient turbulence onset in flows with adverse-pressure gradients while cases without considerable shear stresses, such as constant-pressure flows, remain unaffected.

3 Applications

3.1 Flat-Plate Boundary Layer

The first test case for the new transition modelling approach is the 2D flat-plate boundary layer with constant pressure. As the present method is aimed at modelling Tollmien-Schlichting-type transition, we investigate the experiments of Schubauer & Klebanoff [23] at $Re = 6 \cdot 10^6$ conducted in a low-noise wind tunnel. As in all computations presented in this paper, a second-order central scheme for the mean-flow convection with scalar artificial dissipation as well as low-Mach number preconditioning are applied. Moreover, realistic low-noise conditions are provided by specifying a turbulence intensity of $Tu = 0.1\%$ at the inflow boundaries.

A value of $N_{crit} = 8.5$ is found to match the experimentally observed transition location at about $Re_x = 3 \cdot 10^6$ which defines the location x_0 for the stability analysis for the highest amplified mode f_0 . The Reynolds stresses computed from the eigenfunctions and scaled according to Eq. (10) and (13) as well as the dissipation rate derived from Eq. (12) are depicted in Fig. 5. While original point transition completely suppresses turbulence onset (as described in Sec. 2.2.1), the local input profiles from Fig. 5 prescribed at x_0 enable the ε^h -RSM to compute a skin-friction distribution similar to common “high-Re“ models (see Fig. 6).

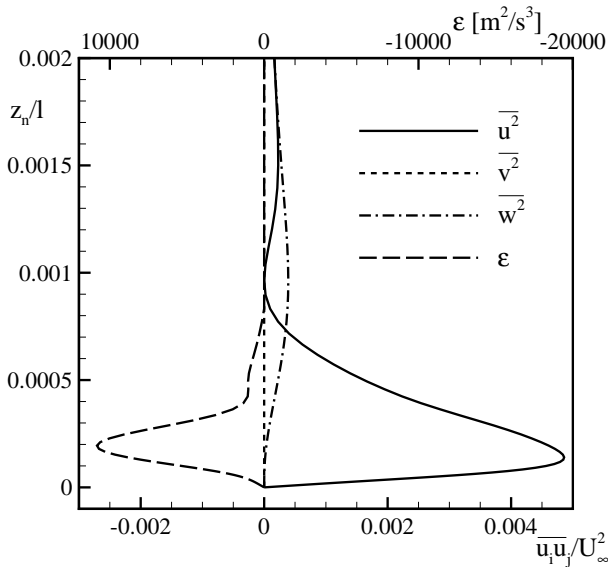


Figure 5: Input profiles of Reynolds stresses and dissipation rate at x_0 computed with the present transition model for the flat-plate flow.

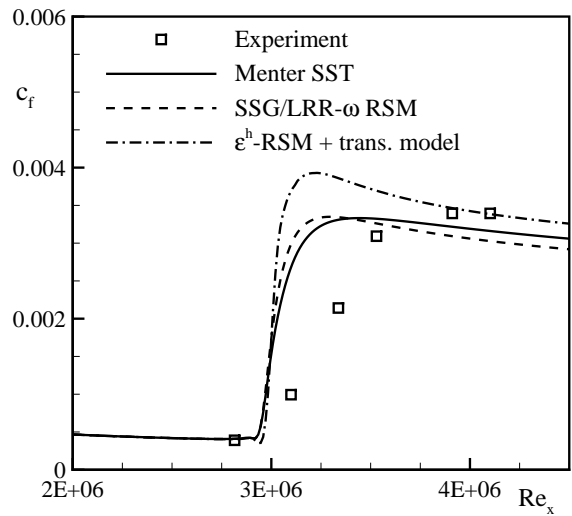


Figure 6: Skin-friction distribution on the flat plate computed with the present transition model for the ε^h -RSM in comparison to experiments and other turbulence models.

The c_f deviations between the three models downstream of transition also occur in fully-turbulent flow cases and are not attributed to the transition modelling. However, compared to the experiment all models compute a too steep rise of c_f at turbulence onset. This is most probably caused by ignoring intermittency in the simulation which is known to primarily affect transitional boundary layers with negative or zero pressure gradients. As most relevant flows in aircraft aerodynamics involve adverse pressure gradients, the phenomenon of intermittency is not addressed at present.

3.2 Boundary Layer with Adverse-Pressure Gradient

As typical transition scenario for aerodynamic flows, the new modelling approach is applied to the calibration case of a boundary layer under adverse pressure gradient as described in Sec. 2.2.4. Based on the results of the stability analysis presented in Figs. 3 and 4, the actual computation with the new transition model for the ε^h -RSM yields the skin-friction distribution depicted in Fig. 7.

While the unmodified point-transition simulation shown for comparison again suppresses turbulence onset and preserves laminar flow, the new model ensures consistent transition and computes the gradient of c_f downstream of turbulence onset in good agreement with DNS. However, the pronounced maximum in

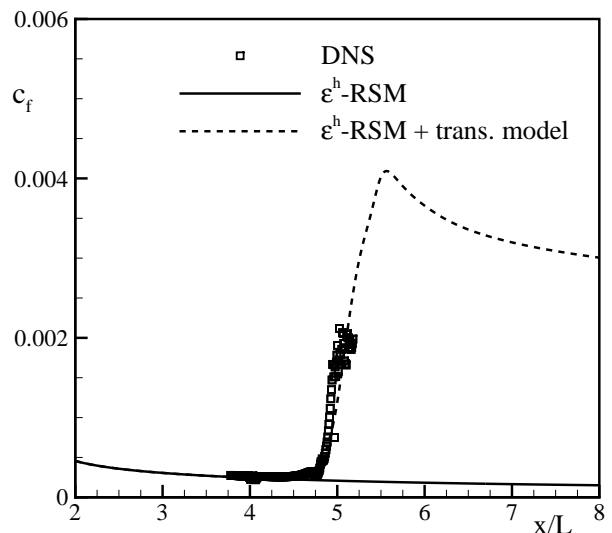


Figure 7: Skin friction in the APG flow computed with the ε^h -RSM and DNS.

c_f cannot be finally judged since no reliable DNS data for the mean skin friction is available in the fully-turbulent region.

3.3 Laminar Separation Bubble on the Airfoil SD7003

As discussed in Sec. 2.2.1 the simulation of transitional flows with laminar separation bubbles, such as the SD7003 airfoil flow at $\alpha = 4^\circ$ and $Re = 60000$, poses a great challenge for any turbulence model applied with point transition. It is therefore a crucial test case for the present transition modelling method in combination with the Low-Re ε^h -RSM.

The computations are performed on a hybrid mesh which is based on a previous grid-refinement study [9]. To analyse the influence of the inflow-turbulence level on the bubble size, which is known to be sensitive from measurements in different wind tunnels, three different critical N factors for transition prediction are applied ($N_{crit} = 7, 8$ and 9).

For $N_{crit} = 7$ and 9 , the Reynolds-stress and dissipation-rate profiles computed from the eigenfunctions at the respective locations x_0 are depicted in Fig. 8. The deviations in the wall-normal stretching and in the magnitude of $\overline{w^2}$ indicate variations in the bubble's shape and size. This

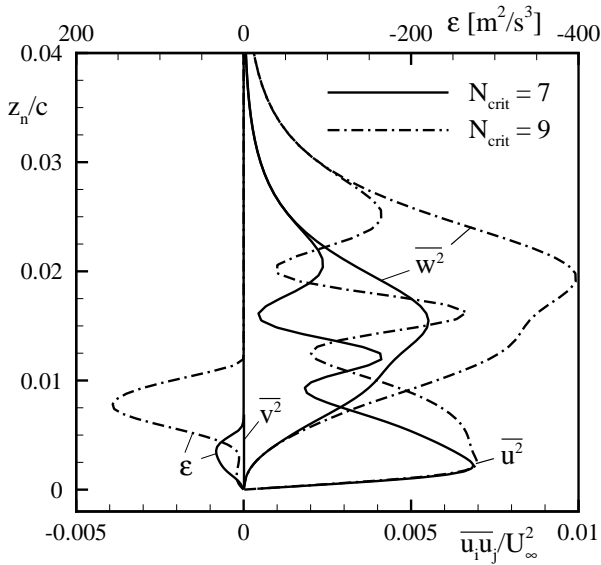


Figure 8: Input profiles of Reynolds stresses and dissipation rate for varying N_{crit} computed with the present transition model for the airfoil SD7003 at $\alpha = 4^\circ$.

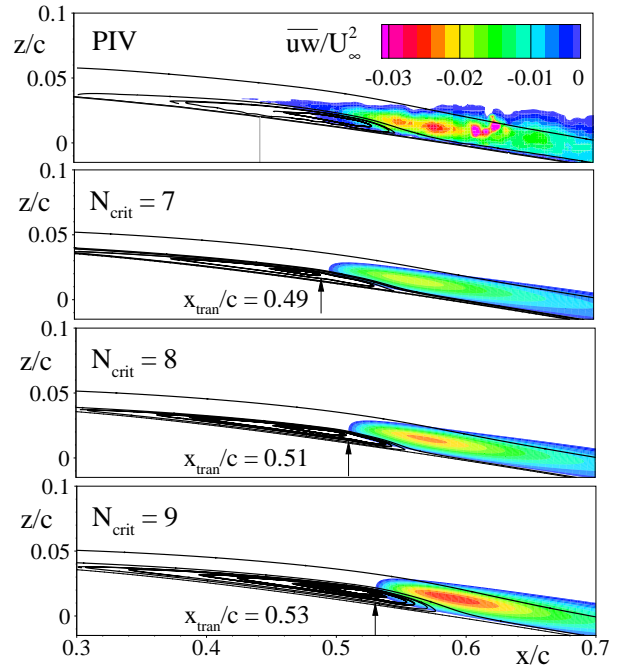


Figure 9: Streamlines and turbulent shear stress on the airfoil SD7003 at $\alpha = 4^\circ$ from experiments [18] and computations with the present transition model for varying N_{crit} .

is confirmed by the flow-field visualizations in Fig. 9 which reveal a clear trend towards a longer, thicker bubble with increased N_{crit} which is accompanied by increased maximum turbulent shear stresses around reattachment. Compared to the PIV results the simulation with $N_{crit} = 8$ agrees well with respect to both the bubble size and the Reynolds-stress distribution, yielding a clear improvement compared to the results obtained from unmodified point transition as described in Sec. 2.2.1.

3.4 3D Flow-Through Nacelle

To assess the present approach for a general 3D flow case it is applied to a stalling flow-through nacelle which was designed by Schulze et al. [24] within the DFG-FOR 1066 project. In previous numerical studies of this case [13] the tendency to inlet separations was found to strongly depend on the parameters of an earlier transition model for the ε^h -RSM [14] which required empirical adjustment of a transitional length. Thus, avoiding this undesired sensitivity constitutes one of the motivations for the present work.

In an exemplary application at near-stall conditions, $\alpha = 20^\circ$, a total of 11 inviscid streamlines are distributed inside the nacelle to resolve the variations in the transition locations and turbulent quantities (see Fig. 10). At the design Reynolds number of $Re = 1.3 \cdot 10^6$ in low-speed conditions, $Ma = 0.15$, the experiments required carefully adjusted transition tripping in order to prevent an undesired laminar leading-edge stall at high angles of attack [13]. To approximate the principal effects of the experimental tripping the critical N factor is iteratively adjusted until the laminar separation bubble in the lower part of the inlet, which was observed in the experiments, is stably reproduced in the simulations. As expected, this is achieved for a comparably low value of $N_{crit} = 4.5$.

In accordance with the circumferential pressure variations visible in Fig. 10 the Reynolds-stress input profiles in Fig. 11 as well as the computed transition locations and skin-friction distributions in Fig. 12 deviate strongly at different circumferential angles Θ : while the boundary layer in the upper section ($\Theta = 0^\circ$) remains attached and undergoes late transition similar to the flat-plate flow (see Sec. 3.1), the lateral and bottom sections at $\Theta = 90^\circ$ and 180° feature the expected laminar separation bubble, resulting in early transition, multiple maxima in the streamwise fluctuation profile and rapidly increasing skin friction after turbulence onset. As de-

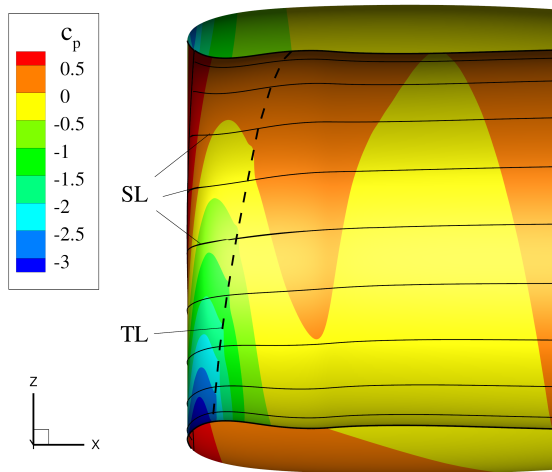


Figure 10: Inviscid streamlines (SL), transition line (TL) and pressure distribution in the flow-through nacelle at $\alpha = 20^\circ$ computed with the present approach.

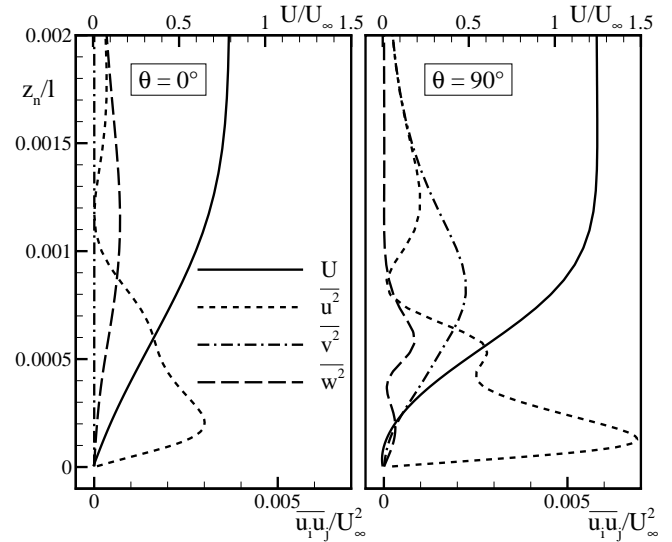


Figure 11: Input Reynolds-stress profiles in different circumferential cut sections in the flow-through nacelle at $\alpha = 20^\circ$ computed with the present approach.

picted in Fig. 13, a moderate variation of N_{crit} with the present model only slightly affects the tendency to separation in the inlet, represented by the level of minimum c_f around $x/c = 0.14$. Thus, compared to the previous approach mentioned above the uncertainties with respect to

the transition model are clearly reduced. Although there exists no detailed experimental data for further validation, the results are broadly in line with expectations and demonstrate the present approach to allow for reliable simulations of 3D flows involving a mixture of different transition scenarios.

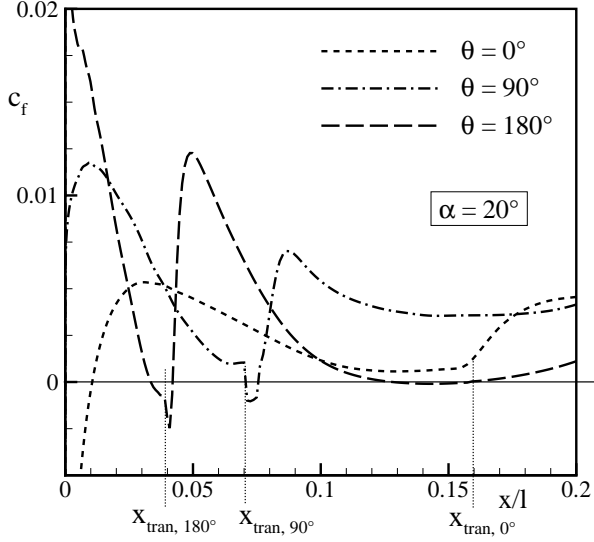


Figure 12: Transition locations and skin friction in different circumferential cut sections in the flow-through nacelle at $\alpha = 20^\circ$ computed with the present approach, $N_{crit} = 4.5$.

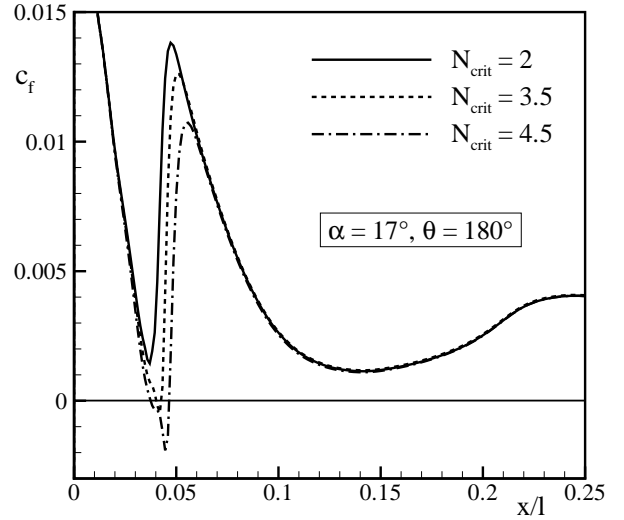


Figure 13: Influence of N_{crit} in the present approach on the tendency to separation in the lower cut section in the flow-through nacelle at $\alpha = 20^\circ$.

4 Conclusion

To improve the classical point-transition method in RANS simulations of aerodynamic flows, a new approach that models Tollmien-Schlichting-type transition has been derived. It incorporates the usually omitted velocity fluctuations at the end of the transitional region. Based on linear stability analysis and calibrated with the aid of DNS data the new method provides realistic Reynolds-stress and dissipation-rate profiles at the transition location and thus clearly enhances the transitional behaviour of the Low-Re ε^h -RSM. Comparison to DNS and experimental data yield improved predictions of boundary-layers with zero- and adverse-pressure gradients and an airfoil flow with a laminar separation bubble, while the applicability to complex 3D flows was demonstrated for a flow-through nacelle near stall conditions.

Despite overall satisfying results, several open questions should be considered. Due to the limited number of suited transitional flow data from DNS and its persistent constraints with respect to the Reynolds number, the assumptions for calibrating the Reynolds-stress magnitudes are not free of doubts. For instance, a Reynolds-number dependency of the scaling of the Reynolds stress cannot be ruled out and might require additional modelling effort, especially at flight Reynolds numbers.

For broad future applications the new method could possibly be combined and validated with other RANS turbulence models as well. Moreover, the method is to be extended to consider crossflow-type transition which plays a dominant role in flows over swept wings.

Acknowledgments

The members of the FOR 1066 research group gratefully acknowledge the support of the "Deutsche Forschungsgemeinschaft DFG" (German Research Foundation) which funded this research.

The computational resources for the simulations of the flow-through nacelle were kindly provided by "The North-German Supercomputing Alliance" (HLRN).

References

- [1] Abu-Ghannam, B.J. and Shaw, R.: "Natural Transition of Boundary Layers-The Effects of Turbulence, Pressure Gradient, and Flow History". *Journal of Mechanical Engineering Science*, Vol. 22, No. 5, 1980, pp. 213 - 228.
- [2] Langtry, R.B. and Menter, F.R.: "Transition Modeling for General CFD Applications in Aeronautics". AIAA 2005-522, 2005.
- [3] Van Ingen, J.L.: "A suggested Semi-Empirical Method for the Calculation of the Boundary Layer Transition Region". Univ. of Delft, Dept. Aerospace Engineering, Delft, The Netherlands, Rep. VTH-74, 1956.
- [4] Arnal D.: "Boundary layer transition: prediction based on linear theory". AGARD-R-793; 1994.
- [5] Schwamborn, D., Gerhold, T., Heinrich, R.: "The DLR TAU-Code: recent applications in research and industry". In: Wesseling P, Onate E, Periaux, J, editors. European conference on computational fluid dynamics, ECCOMAS CFD 2006; 2006.
- [6] Krimmelbein, N., Radespiel, R.: "Transition prediction for three-dimensional flows using parallel computation". *Computers & Fluids*, Vol. 38, No. 1, pp. 121-136, Jan. 2009.
- [7] Krumbein, A.: "Automatic Transition Prediction and Application to 3D Wing Configurations". AIAA-2006-914, 2006.
- [8] Dhawan, S., Narasimha, R.: "Some properties of boundary layer flow during the transition from laminar to turbulent motion". *Journal of Fluid Mechanics*, Vol. 3, 1958, pp. 418-436.
- [9] Windte, J., Scholz, U., Radespiel, R.: "Validation of the RANS-simulation of laminar separation bubbles on airfoils". *Aerospace Science and Technology*, Vol. 10, No. 6, 2006, pp. 484-494.
- [10] Patel, V.C., Rodi, W., and Scheurer, G.: "Turbulence Models for Near-Wall and Low-Reynolds-Number Flows: A Review". AIAA. *Journal* 23, 1308-1319, 1985.
- [11] Rumsey, C.L., Pettersson Reif, B.A., Gatski, T.B.: "Arbitrary Steady-State Solutions with the K- ϵ Model". AIAA *Journal*, Vol. 44, No. 7, pp. 1586-1592, 2006.
- [12] Jakirlić, S., Hanjalić, K.: "A new approach to modelling near-wall turbulence energy and stress dissipation". *J. Fluid Mech*, Vol. 459, pp. 139-166, 2002.

- [13] Probst, A., Schulze, S., Radespiel, R., Kähler, C.J.: “Numerical and Experimental Investigation of a Stalling Flow-Through Nacelle”. To appear in: *New Results in Numerical and Experimental Fluid Mechanics VII, Notes on Numerical Fluid Mechanics and Multidisciplinary Design (NNFM)*, Vol. 112, Springer, 2010.
- [14] Probst, A., Radespiel, R.: “Implementation and Extension of a Near-Wall Reynolds-Stress Model for Application to Aerodynamic Flows on Unstructured Meshes”. AIAA-2008-770, 2008.
- [15] Menter, F. R.: “Zonal Two Equation $k-\omega$ Turbulence Models for Aerodynamic Flows”. AIAA Paper 93-2906, 1993.
- [16] Wilcox, D.C.: “Turbulence Modelling for CFD”. Second edition, DCW Industries, La Canada, 1998.
- [17] Schlichting, H., Gersten, K.: “Boundary Layer Theory”. Springer, New York, 2000.
- [18] Ol, M.V., McAuliffe, B.R., Hanff, E.S., Scholz, U., Kähler, C.J.: “Comparison of Laminar Separation Bubble Measurements on a Low Reynolds Number Airfoil in Three Facilities”. AIAA Paper 2005-5149, 2005.
- [19] Schrauf G.: “LILO 2.1. User’s guide and tutorial”. GSSC technical report 6, 2006.
- [20] Mack, L.M.: “Transition and laminar instability”. Jet Propulsion Laboratory Publication 77-15, Pasadena, 1977.
- [21] Rist, U.: “Zur Instabilität und Transition in laminaren Ablöseblasen”. Habil.-Schr., Universität Stuttgart, Shaker Verlag, Aachen, 1999.
- [22] Kloker, M.J., Fasel, H.F.: “Direct numerical simulation of boundary layer transition with strong adverse pressure gradient“. In: R. Kobayashi (Ed.): ”Proc. IUTAM-Symp. Laminar-Turbulent Transition, Sept. 5-9, 1994, Sendai, Japan“, Springer-Verlag, 481 - 488, 1995.
- [23] Schubauer, G.B., Klebanoff, P.S.: “Contributions on the Mechanics of Boundary-Layer Transition”. NACA Technical Report 1289, 1956.
- [24] Schulze, S., Kähler, C., Radespiel, R.: “On the Comparison of Stalling Flow-Through a Nacelles and Powered Inlets at Take-Off Conditions”. 1st CEAS European Air and Space Conference, Berlin, Germany, 10-13 September, 2007.